

Kagóme Cobalt(II)-Organic Layers as Robust Scaffolds for Highly Efficient Photocatalytic Oxygen Evolution

Jiaheng Xu,^[a] Zhi Wang,^[a] Wenguang Yu,^[b] Di Sun,*^[a] Qing Zhang,^[b] Chen-Ho Tung,^[a] and Wenguang Wang*^[a]

Two Kagóme cobalt(II)-organic layers of $[\text{Co}_3(\mu_3\text{-OH})_2(\text{bdc})_2]_n$ (**1**) and $[\text{Co}_3(\mu_3\text{-OH})_2(\text{chdc})_2]_n$ (**2**) ($\text{bdc}=\text{o-benzenedicarboxylate}$ and $\text{chdc}=1,2\text{-cyclohexanedicarboxylate}$) that bear bridging OH^- ligands were explored as water oxidation catalysts (WOCs) for photocatalytic O_2 production. The activities of **1** and **2** towards H_2O oxidation were assessed by monitoring the *in situ* O_2 concentration versus time in the reaction medium by utilizing a Clark-type oxygen electrode under photochemical conditions. The oxygen evolution rate (R_{O_2}) was $24.3 \mu\text{mol s}^{-1} \text{g}^{-1}$ for **1** and $48.8 \mu\text{mol s}^{-1} \text{g}^{-1}$ for **2** at pH 8.0. Photocatalytic reaction studies show that **1** and **2** exhibit enhanced activities toward the oxidation of water compared to commercial nanosized Co_3O_4 . In scaled-up photoreactions, the pH value of the reaction medium decreased from 8.0 to around 7.0 after 20 min

and the O_2 production ceased. Based on the amounts of the sacrificial oxidant ($\text{K}_2\text{S}_2\text{O}_8$) used, the yield of O_2 produced is 49.6% for **2** and 29.8% for **1**. However, the catalyst can be recycled without a significant loss of catalytic activity. Spectroscopic studies suggest that the structure and composition of recycled **1** and **2** are maintained. In isotope-labeling H_2^{18}O (97% enriched) experiments, the distribution of $^{16}\text{O}^{16}\text{O}/^{16}\text{O}^{18}\text{O}/^{18}\text{O}^{18}\text{O}$ detected was 0:7.55:92.45, which is comparable to the theoretical values of 0.09:5.82:94.09. This work not only provides new catalysts that resemble ligand-protected cobalt oxide materials but also establishes the significance of the existence of OH^- (or H_2O) binding sites at the metal center in WOCs.

Introduction

The photocatalytic oxidation of water to produce O_2 , protons, and electrons is an attractive reaction with which to capture solar energy in both sustainable energy storage and transformation.^[1–5] The released protons and electrons can potentially be utilized to synthesize various chemicals, and for example, i) to produce H_2 as a fuel directly;^[6] ii) to reduce CO_2 to HCOOH , CO , or CH_3OH ;^[7] and iii) to store as a hydride ($\text{H}^- \leftrightarrow \text{H}^+ + 2\text{e}^-$) in reduction products such as dihydropyridine derivatives for further transformation.^[8] To achieve this multi-step e^-/H^+ transfer reaction, a natural oxygen evolution center uses an intact Mn_4CaO_5 cluster surrounded by $\mu\text{-O}$ and $\mu\text{-OH}$ ligands in photosystem II (PS II).^[9] However, in an artificial cycle, photocatalytic water oxidation to produce O_2 is still a challenge.

In recent years, efforts have focused on the development of heterogeneous^[10] and homogenous^[11] water oxidation catalysts (WOC). WOCs based on complexes of Ru,^[12–18] Ir,^[19–24] Mn,^[25–27] Cu,^[28–30] Co,^[31–38] and Fe^[39–44] with well-defined structures have provided mechanistic insights into the critical steps to lead to O=O bond formation. For example, one crucial intermediate in the process of O=O bond formation is the high-valence metal oxo ($\text{M}-\text{O}$) species, which is generated by a multistep proton-coupled electron transfer (PCET) oxidation of metal hydroxyl ($\text{M}-\text{OH}$) or metal aqua ($\text{M}-\text{OH}_2$) units on the WOCs. We are especially interested in photo-WOCs based on abundant metals, which require systems with high “photo-robustness”.^[45] Recently, Co- and Ni-based polyoxometalates (POMs) were found to perform well for photocatalytic O_2 production.^[31, 46–49] However, these POMs degraded into heterogeneous metal oxides or hydroxyl oxides in some cases.^[8b, 50] In contrast to molecular WOCs, heterogeneous catalysts such as metal oxides have high turnover frequencies and robustness but their characterization is challenging, which inhibits the optimization of the catalyst.^[51]

Metal-organic frameworks (MOFs) provide suitable scaffolds for photo-WOCs because of their well-organized structures, multiple metal centers with redox activity, and high surface area for the reaction to occur. As heterogeneous WOCs they are photo-robust and recycled easily.^[52] Specifically, MOFs that consist of $\mu\text{-O}$ and $\mu\text{-OH}$ ligands are potential sites for the activation of H_2O to lead to O_2 evolution. To date, however, examples of MOFs-based photo-WOCs are rare, especially those

[a] J. Xu, Z. Wang, Dr. D. Sun, Dr. C.-H. Tung, Dr. W. Wang
Key Lab of Colloid and Interface Chemistry, Ministry of Education
School of Chemistry and Chemical Engineering
Shandong University
Jinan, 250100 (P. R. China)
E-mail: wwg@sdu.edu.cn
dsun@sdu.edu.cn

[b] W. Yu, Dr. Q. Zhang
Dalian Institute of Chemical Physics
Chinese Academy of Sciences
457 Zhongshan Road, Dalian 116023 (China)

Supporting Information and the ORCID identification number(s) for the author(s) of this article can be found under <http://dx.doi.org/10.1002/cssc.201600101>.

with low-cost metals.^[53] Very recently, Mao et al. reported photocatalytic O₂ production by layered organic cobalt phosphonates as heterogeneous catalysts for H₂O oxidation.^[54] The oxo-bridged metal centers in these cobalt(II) phosphonates is thought to facilitate water oxidation. Herein, we report two new layered cobalt(II) dicarboxylates as photo-WOCs. The materials [Co₃(μ₃-OH)₂(bdc)₂]_n (**1**) and [Co₃(μ₃-OH)₂(chdc)₂]_n (**2**) (bdc= *o*-benzenedicarboxylate and chdc= 1,2-cyclohexanedicarboxylate) have the advantage that they are assembled readily in good yield and high purity. Importantly these new materials exhibit a high activity for photocatalytic water oxidation (Scheme 1). The catalytic activities of

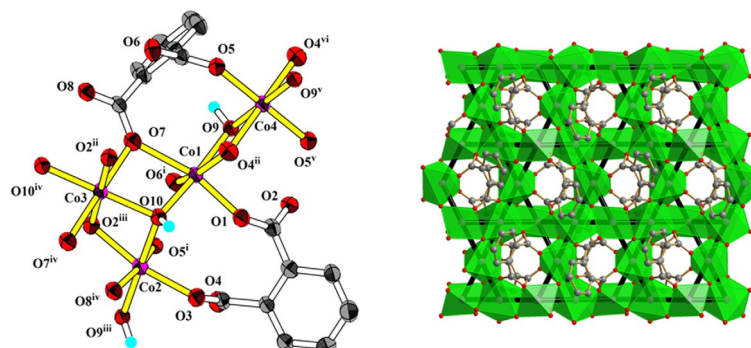
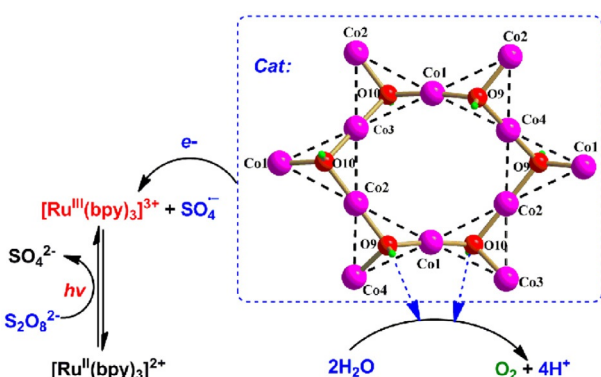


Figure 1. ORTEP view of the coordination environment of Co^{II} in the structure of **1** (left) and polyhedral representation of the distorted Kagomé lattice of **1** (right).



Scheme 1. Schematic photocatalytic O₂ production in a three-component system: [Ru^{III}(bpy)₃]³⁺ (sensitizer), S₂O₈²⁻ (sacrificial oxidant), and catalyst (Cat.). For Cat.: ball-and-stick view of the arrangement of Co^{II} in the synthetic cobalt(II) dicarboxylate layer of **1** (dicarboxylate ligands are omitted for clarity, details are shown in Figure 1).

these two WOCs were evaluated using a Clark-type oxygen electrode under photochemical conditions. The difference in O₂ production performance between **1** and **2** provides an opportunity to correlate the structure with the activity. Our work provides not only a new family of WOCs but also valuable information about the potential sites in such catalysts that are activators of water oxidation.

Results and Discussion

Synthesis and structures of **1** and **2**

Compound **1** was synthesized from Co(NO₃)₂·6H₂O, 1-aminotetrazole, and *o*-benzenedicarboxylic acid in H₂O/CH₃OH mixed solvent at 180 °C, and **2** was prepared according to a modified method similar to that described in the literature.^[55] Compounds **1** and **2** were isolated as fine pink and purple crystals, respectively, some of which were suitable for single-crystal XRD analysis.

In the structure of **1**, each asymmetric unit contains two bdc²⁻ ligands, two μ₃-OH groups, and four Co^{II} atoms. Two of the Co^{II} atoms (Co3 and Co4) are located at the crystallographic inversion center (Figure 1). Each Co^{II} atom is in a slightly dis-

torted octahedral geometry coordinated by four O_{carboxylate} atoms (Co—O, 2.011(6)–2.106(6) Å) and two μ₃-OH groups (Co—O, 2.115(7)–2.342(7) Å). Co1 and Co2 are connected to two different hydroxyl groups, and Co3 and Co4 are coordinated by the two same symmetry-related μ₃-OH groups (O10 for Co3 and O9 for Co4), which create two different triangles (Co1Co2Co3 and Co1Co2Co4) in **1**. Three Co atoms in these two triangles are consolidated by two different μ₃-OH groups, O10 for Co1Co2Co3 and O9 for Co1Co2Co4 (Scheme 1). The Co...Co separation in these two triangles is in the range of 3.11–3.53 and 3.09–3.52 Å, respectively. The two triangles are corner-shared to furnish a distorted Kagomé lattice that runs along the bc plane (Figure 1). All the Co atoms are located in the vertices of the Kagomé lattice. The bdc²⁻ ligand is almost perpendicular to the cobalt(II) hydroxide layer. Benzene rings of bdc²⁻ act as an organic skin to provide protection up and down the resultant layer. The layers are packed along the *a* direction by van der Waals interactions with an interlayer distance of 10.2 Å.

Complex **2** has the same ratio of Co^{II} atoms, hydroxyl groups, and dicarboxylate groups (3:2:2) as **1** (Figure S1). The detailed structure of **2** has been described previously.^[55] Notably, not all Co^{II} atoms are in the six-coordinated octahedral geometry. Co1 is coordinated by two O atoms from two carboxylate ligands and the O atoms from two hydroxyl groups to give a distorted CoO₄ tetrahedron, and the other two Co^{II} atoms are in the usual octahedral geometry. As a result of the tetrahedral Co1 atom in **2**, the 2D layer exhibits a much more distorted Kagomé lattice in contrast to that of **1**, in which the tetrahedral Co1 is in a corner-shared position and forms the Co1Co2Co3 triangle with μ₃-OH groups. The interlayer distance in **2** is increased to 13.6 Å, which is one of the most important factors to govern its outstanding O₂ evolution performance as shown in the following section.

Photochemical O₂ production monitored using a Clark electrode

The catalytic activity of **1** and **2** for O₂ production was evaluated using a Clark-type oxygen electrode system under photochemical conditions. A 2.0 mL degassed borate buffer solution (pH 8.0) that contained crystals of **1** or **2** (2 mg), 3.0 mM

$K_2S_2O_8$, and 0.4 mM $[Ru(bpy)_3]^{2+}$ ($bpy =$ bipyridine) was irradiated using a 450 nm light-emitting diode (LED) lamp. The amount of evolved O_2 dissolved in solution versus time (t) was measured *in situ* using a Clark electrode. Compounds **1** and **2**

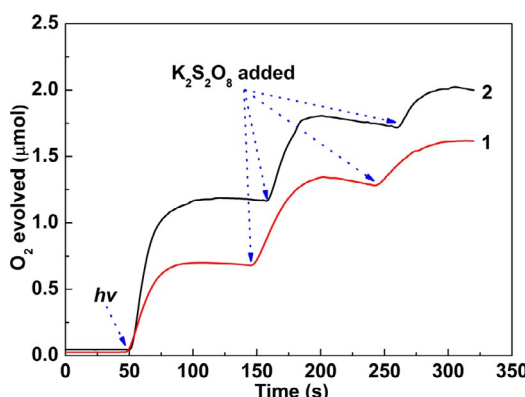


Figure 2. O_2 evolution catalyzed by **1** (red) and **2** (black) under photochemical conditions: 2 mg catalysts, 0.4 mM $[Ru(bpy)_3]^{2+}$, 3.0 mM $K_2S_2O_8$, 0.2 M borate buffer (2.0 mL, initial pH 8.0), and with a 450 nm LED lamp light source.

show the same tendency to produce O_2 upon the irradiation of the reaction medium (Figure 2). After irradiation for ≈ 2 s, O_2 evolution starts, and the amount of O_2 increases almost linearly during the first 20 s. Then, the oxygen evolution rates (R_{O_2} , $\mu\text{mol s}^{-1} \text{g}^{-1}$) declined over the next 10 s, and subsequently, oxygen generation ceased gradually. This photocatalytic O_2 production system recovered if fresh $K_2S_2O_8$ buffer solution was added. For instance, the total amount of O_2 in the solution of **1** increased from 0.7 μmol (first step in Figure 2, $R_{O_2} = 12.6 \mu\text{mol s}^{-1} \text{g}^{-1}$) to 1.4 μmol (second step, $R_{O_2} = 9.2 \mu\text{mol s}^{-1} \text{g}^{-1}$). Although the O_2 production continued, the rate of production decreased ($R_{O_2} = 4.4 \mu\text{mol s}^{-1} \text{g}^{-1}$) after an extra equivalent of $K_2S_2O_8$ was added. Compound **2** shows higher levels of O_2 production, and the total amount of O_2 increased from 1.2 μmol (first step in Figure 2, $R_{O_2} = 27.1 \mu\text{mol s}^{-1} \text{g}^{-1}$) to 1.8 μmol (second step, $R_{O_2} = 12.4 \mu\text{mol s}^{-1} \text{g}^{-1}$) and 2.0 μmol (third step, $R_{O_2} = 6.5 \mu\text{mol s}^{-1} \text{g}^{-1}$).

Further studies revealed that the initial R_{O_2} was affected by the concentrations of both $[Ru(bpy)_3]^{2+}$ and $[S_2O_8]^{2-}$ and the amount of catalyst (Figures S3–S6). For example, if the concentration of $[Ru(bpy)_3]^{2+}$ was increased from 0.1 to 1.0 mM, the R_{O_2} increased almost linearly from 1.75 to 18.35 $\mu\text{mol s}^{-1} \text{g}^{-1}$ (Figure S4). Several control experiments indicated that **1** and **2** are indispensable for O_2 production. In the absence of **1** or **2**, under otherwise identical conditions, no O_2 was measured in the degassed solution. In contrast to the same amount of free Co^{2+} provided by cobalt acetate or commercial Co_3O_4 (≈ 30 nm size) particles, **1** and **2** are much more active (Figure S7).

The catalysts operate optimally, and the highest level of O_2 was produced at pH 8.0. At pH 8.0 and with 1.0 mM $[Ru(bpy)_3]^{2+}$ and 9.0 mM $K_2S_2O_8$, the plateau amount of O_2 reached 1.7 μmol for **1** and 2.3 μmol for **2**. Compound **2** is more active with respect to O_2 production than **1**, reflected by their R_{O_2} values ($48.8 \mu\text{mol s}^{-1} \text{g}^{-1}$ for **2** vs. $24.3 \mu\text{mol s}^{-1} \text{g}^{-1}$ for **1**). A decrease of the pH to 7.4 or an increase to 9.0, resulted in a decrease of R_{O_2} . The effect of pH on R_{O_2} for **1** is 24.3 (pH 8.0) > 16.9 (pH 9.0) > $12.5 \mu\text{mol s}^{-1} \text{g}^{-1}$ (pH 7.4), and 48.8 (pH 8.0) > 21.4 (pH 9.0) > $15.3 \mu\text{mol s}^{-1} \text{g}^{-1}$ (pH 7.4) for **2** (Figure 3). Compounds **1** and **2** are much more active than commercial Co_3O_4 particles (≈ 30 nm size; Figure S7 and Table 1). Compounds **1** and **2** can be recycled and remain active for several cycles (Figure S9). The IR spectra recorded for the recycled samples match well with those of the fresh crystals (Figure S11).

Scaled-up photocatalytic O_2 production

To determine the highest amount of O_2 produced, we conducted a scaled-up reaction in a Pyrex tube and quantified the O_2 production by GC analysis. Typically, 10.0 mL of borate solution

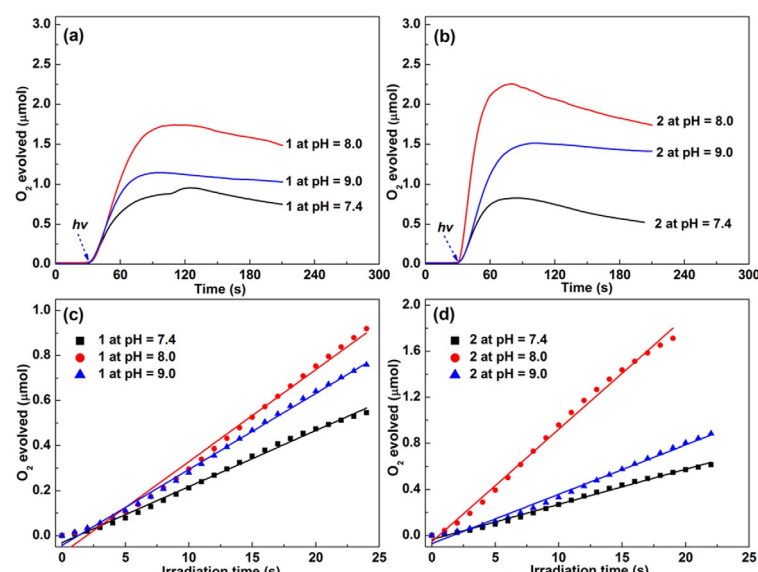


Figure 3. Results of O_2 evolution for a) **1** and b) **2** at different pH values, and the fitting curve of the initial linear parts of the curves of c) **1** and d) **2**. Conditions: 1.0 mM $[Ru(bpy)_3]^{2+}$, 9.0 mM $K_2S_2O_8$, 0.2 M borate buffer (2.0 mL, initial pH 7.4, 8.0, 9.0), and a 450 nm LED lamp light source.

Table 1. O_2 evolution, turnover number (TON), and turnover frequency (TOF) of **1**, **2**, and Co_3O_4 measured using a Clark-type oxygen electrode.

Catalyst	O_2 evolved [μmol]	TON	$TOF \times 10^3 [\text{s}^{-1}]$
1	1.78	0.96	14
2	2.28	1.26	20
Co_3O_4	0.41	0.049	0.77

Conditions: 1.0 mM $[Ru(bpy)_3]^{2+}$, 9.0 mM $K_2S_2O_8$, 0.2 M borate buffer (2.0 mL, initial pH 8.0), and a 450 nm LED lamp light source.

(pH 8.0) that contained **1** or **2** (1.0 mg mL^{-1}), $[\text{Ru}(\text{bpy})_3]^{2+}$ (1.0 mM), and $\text{K}_2\text{S}_2\text{O}_8$ (9.0 mM) was photolyzed using a 450 nm LED lamp. The produced O_2 in the headspace was analyzed using a GC equipped with a 5 \AA molecular sieve column and a thermal conductivity detector with Ar as the carrier gas and methane as the internal standard. Contamination of the headspace caused by air in the degassed samples was nullified by measurement of the N_2 peak using GC.

The O_2 produced by **1** and **2** over time is shown in Figure 4. Remarkably, both **1** and **2** are extremely active toward water

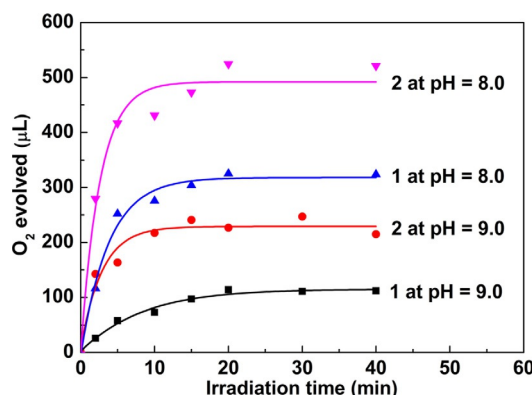


Figure 4. O_2 evolution results from scaled-up photocatalytic reactions for **1** and **2** at different pH conditions: 1.0 mg mL^{-1} catalysts, 1.0 mM $[\text{Ru}(\text{bpy})_3]^{2+}$, $9.0 \text{ mM K}_2\text{S}_2\text{O}_8$, 0.2 M borate buffer (10.0 mL , initial pH 8.0, 9.0), with a 450 nm LED lamp light source.

oxidation, consistent with the results obtained using the Clark-type electrode. Independent of O_2 dissolved in the solution, the highest amount of O_2 after 20 min photolysis was 0.3 mL for **1** and 0.5 mL for **2** at pH 8.0. Based on the amounts of $\text{K}_2\text{S}_2\text{O}_8$ used, the yields of O_2 are 29.8% for **1** and 49.6% for **2**. Notably, the pH value decreases from 8.0 to 7.1 after the photoreaction. Although the O_2 evolution ceased, the samples can be recycled and remained active for several further cycles (Figure S10). We found that recycled **1** and **2** essentially retain their activities. IR spectra and powder XRD patterns of recycled **1** and **2** confirm that the layered frameworks are maintained after the reaction (Figures S11 and S12). The X-ray photoelectron spectroscopy (XPS) spectra of the recycled samples are similar to those of the as-prepared samples (Figures S13 and

S14), which indicates that the surface compositions also survive well. Moreover, in contrast to the same amount of free Co^{2+} provided by cobalt acetate or commercial Co_3O_4 particles ($\approx 30 \text{ nm}$ size), **1** and **2** are much more active, consistent with the results obtained using the Clark-type electrode (Figure S8 and Table S1).

Electrochemistry

To further elucidate the catalytic properties of **1** and **2**, electrochemical experiments were conducted. Cyclic voltammetry (CV) and linear sweep voltammetry (LSV) of **1**, **2**, and Co_3O_4 nanoparticles ($\approx 30 \text{ nm}$) were performed using a three-electrode arrangement in 0.2 M borate buffer at pH 8.0. The CVs of **1** and **2** display an irreversible oxidation wave at around 0.90 V [vs. the normal hydrogen electrode (NHE)] and, subsequently, an onset catalytic wave (Figure 5a). The oxidation process is attributed to $\text{Co}^{II}/\text{Co}^{III}$ in the layers, which is more negative than the 1.12 V of that in Co_3O_4 . The overpotential to obtain the current density of 1 mA cm^{-2} of **1**, **2**, and Co_3O_4 is 425, 412, and 622 mV , respectively (Figure 5b). These observations are consistent with the results of photocatalytic O_2 production, namely, that **1** and **2** have higher activities than Co_3O_4 . The stability of **1** and **2** during electrocatalytic water oxidation was tested by performing continuous CV scans (Figure S15). We propose that a $\text{Co}^{IV}=\text{O}$ active species was generated, followed by water nucleophilic attack to form CoOOH , a similar active catalytic species exists in a water oxidation system catalyzed by nickel porphyrin.^[56] The moderate overpotential of **1** and **2** may result from their layered carboxylate framework,^[57] but further work is required to explore details of such structure–property relationships.

Isotope-labeled H_2^{18}O oxidation

To prove that the evolved O_2 resulted from the photocatalyzed oxidation of water, an isotope-labeling experiment was performed using H_2^{18}O (97% enriched) and **2** as the catalyst. The resulting gas samples were analyzed by MS. The results of the isotopic oxygen distribution after the elimination of $^{32}\text{O}_2$ contamination of the headspace caused by air in the degassed samples are shown in Figure 6. The distribution of $^{16}\text{O}^{16}\text{O}$ / $^{16}\text{O}^{18}\text{O}$ / $^{18}\text{O}^{18}\text{O}$ observed in the experiments was 0:7.55:92.45, which matches the theoretical value of 0.09:5.82:94.09. These

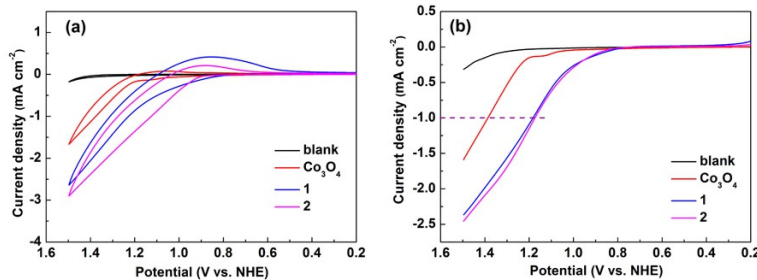


Figure 5. a) CV and b) LSV curves of **1**, **2**, and Co_3O_4 in 0.2 M borate buffer (pH 8.0). Conditions: scan rate: 20 mVs^{-1} ; glassy carbon working electrode (catalyst loading: 1.12 mg cm^{-2}), Ag/AgCl (3.0 M KCl) reference electrode, and Pt wire counter electrode.

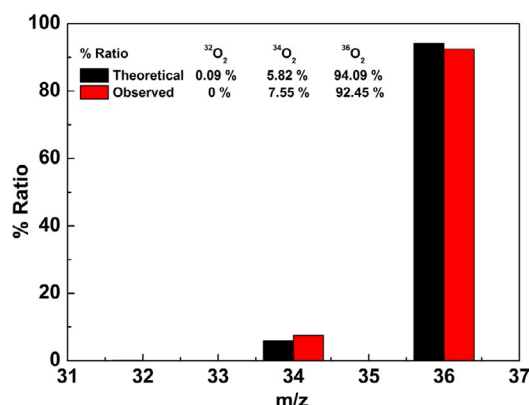


Figure 6. Comparison of the theoretical and observed ratio of $^{32}\text{O}_2$, $^{34}\text{O}_2$, and $^{36}\text{O}_2$ evolved from the isotope-labeling water oxidation experiment using H_2^{18}O (97% enriched).

observations indicate that the O_2 evolved was from H_2O caused by photocatalyzed water oxidation.

The high yield of $^{34}\text{O}_2$ implies that $\mu\text{-OH}$ binding sites in the cobalt(II) carboxylate layers are responsible for the catalytic O_2 evolution. In the cases of Co-Pi^[32,58] (Pi=phosphate) and Co₄O₄(OAc)₄Py₄ (OAc=acetate, Py=pyridine),^[59] the Co^{IV}(O) active species was generated by PCET oxidation of Co^{III}-OH units in the precursors. We propose that a similar Co^{IV}(^{16}O) species is generated in our photocatalytic reactions. The oxidative quenching of excited $^*[\text{Ru}^{\text{II}}(\text{bpy})_3]^{2+}$ by $\text{S}_2\text{O}_8^{2-}$ affords $[\text{Ru}^{\text{III}}(\text{bpy})_3]^{3+}$ as a strong oxidant ($E_{\text{red}} = 1.05 \text{ V}$ vs. Ag/AgCl) and the $\text{SO}_4^{\cdot -}$ radical ($E_{\text{red}} = 2.1 \text{ V}$).^[60,61] The successive oxidation of Co^{II}-OH in **1** or **2** produces the Co^{IV}(^{16}O) species and achieves Co^{IV}($^{16}\text{O}-^{18}\text{OH}$) generation, which under basic conditions releases $^{34}\text{O}_2$. These steps require the highly oxidative $\text{SO}_4^{\cdot -}$ radical. If K₂S₂O₈ was replaced by other sacrificial oxidants such as AgNO₃ or FcBF₄, no O_2 was produced as monitored using the Clark-type oxygen electrode. Compared with the catalytic process of Co₃O₄,^[62] the structural characteristics of **1** and **2** seem to facilitate water oxidation, but further work is required to probe the details of such structure–property relationships.

Conclusions

We have developed two Kagóme cobalt(II) metal hydroxo carboxylate layered compounds that function as water oxidation photocatalysts for the conversion of water into O_2 . These results were verified by *in situ* monitoring using a Clark-type oxygen electrode as well as GC analysis. Isotope-labeling H₂¹⁸O (97% enriched) experiments are consistent with a direct role of the $\mu\text{-OH}$ sites in the O_2 evolution pathway. The catalytic activity of the layers was enhanced by changing the *o*-benzenedicarboxylate ligand to *trans*-1,2-cyclohexanedicarboxylate. This change of the organic ligand increases the interlayer distance by 3.4 Å. Photocatalytic reaction studies show that **1** and **2** possess enhanced activities toward the oxidation of water compared to commercial nanosized Co₃O₄. Further work is required to further probe the details of such structure–property relationships. This work not only provides new catalysts that resemble ligand-protected cobalt oxide materials but also es-

tablishes the significance of the existence of OH⁻ (or H₂O) binding sites at the metal center in water oxidation catalysts.

Experimental Section

Materials and methods

Co(NO₃)₂·6H₂O, *o*-benzenedicarboxylic acid, 1,2-cyclohexanedicarboxylic acid, [Ru(bpy)₃]Cl₂·6H₂O, K₂S₂O₈, H₃BO₃, and Na₂B₄O₇ were purchased from Acros. Nafion perfluorinated resin solution (5 wt%) was purchased from Sigma-Aldrich. ¹⁸O-enriched normalized water (H₂¹⁸O, 97%) was purchased from Shanghai Research Institute of Chemical Industry. Compound **2** was prepared according to a published procedure.^[55] The amount of evolved O_2 dissolved in solution was measured *in situ* using a standard Clark-type oxygen electrode (Hansatech Instruments). The total amount of evolved O_2 was quantified using a Techcomp 7890 II GC equipped with a 5 Å molecular sieve column with Ar as the carrier gas and thermal conductivity detector. FTIR spectra were obtained using a PerkinElmer FTIR Spectrometer Spectrum Two in the range of 4000–450 cm⁻¹. Powder XRD patterns were obtained using a Rigaku D/MAX 2200PC diffractometer equipped with a graphite monochromator and CuK α radiation ($\lambda = 1.5418 \text{ \AA}$) in the range of $2 < 2\theta < 50^\circ$. XPS was performed using an Omicron (ESCA⁺) spectrometer, using an AlK α X-ray source (1486.6 eV) equipped with a flood gun. Binding energies (BEs) were calibrated using the C 1s band (BE = 284.7 eV). Electrochemical measurements (CV and LSV) were performed using a CHI 760e electrochemical workstation (Shanghai Chen Hua Instrument Co., Ltd) with a conventional three-electrode arrangement. The isotope-labeling experiment was performed using a mass spectrometer (MID, model; Omnistar/quadrupole mass analyzer; Pfeiffer Vacuum) using He as the carrier gas (30 mL min⁻¹ flow).

Synthesis of **1**

A mixture of Co(NO₃)₂·6H₂O (0.1 mmol, 29.0 mg), *o*-benzenedicarboxylic acid (0.1 mmol, 16.6 mg), 1-aminotetrazole (0.1 mmol, 8.5 mg), and CH₃OH/H₂O (5 mL, 1:1 v/v) was heated to 180 °C for 10 h in a 25 mL Teflon-lined reaction vessel, kept at 180 °C for 50 h, and then cooled slowly to 30 °C in 13 h. Pink needle-like crystals of **1** were isolated by filtration, washed with EtOH, and dried in air. IR (KBr pellets): $\bar{\nu} = 3605(\text{w}), 1573(\text{m}), 1473(\text{m}), 1373(\text{s}), 1143(\text{m}), 796(\text{s}), 766(\text{s}), 727(\text{s}), 635(\text{s}) \text{ cm}^{-1}$; elemental analysis calcd (%) for Co₃C₁₆O₁₀H₁₀: C 35.65, H 2.02; found: C 35.55, H, 2.02.

Photocatalytic oxygen evolution measured using a Clark-type oxygen electrode

The amount of evolved O_2 dissolved in solution was measured *in situ* using a standard Clark-type oxygen electrode (Hansatech Instruments), the electrode was calibrated following a standard procedure before the measurements. Typically, each component was mixed in 2.0 mL buffer solution, and the solution was degassed with Ar for 30 min before measurement. The degassed solution was then irradiated using a 450 nm LED lamp, and the amount of O_2 evolved in solution was measured *in situ*.

Photocatalytic oxygen evolution measured using GC

The total amount of evolved O_2 was quantified using GC using a Techcomp 7890 II GC with Ar as the carrier gas and a 5 Å molecular sieve column to separate O_2 , N_2 , and CH_4 . The gases were de-

tected using a thermal conductivity detector. Typically, a Pyrex tube was filled with borate buffer solution (10.0 mL, 0.2 M) that contained the catalyst (1.0 mg mL⁻¹), [Ru(bpy)₃]²⁺ (1.0 mM), and K₂S₂O₈ (9.0 mM). Then the tube was sealed with a rubber plug, and the junction between the tube and the rubber plug was sealed with wax. Subsequently, the tube was flushed with Ar for 60 min to remove the residual air. After degassing, CH₄ (200 µL) was injected into the tube as the internal standard. The tube was photolyzed using a 450 nm LED lamp. After photolysis, 200 µL of the gas in the headspace was sampled using a Hamilton (1750 SL) gas-tight microliter syringe and then analyzed by GC. Contamination of the headspace caused by air in the degassed sample was nullified by measurement of the N₂ peak.

Electrochemical measurements

CV and LSV were performed in 0.2 M borate buffer (pH 8.0) using a conventional three-electrode arrangement: Ag/AgCl (3.0 M KCl) as the reference electrode, Pt wire as the counter electrode, and a modified glassy carbon electrode as the working electrode. The modified glassy carbon electrode was prepared as follows: a glassy carbon electrode was covered with 15 µL of an ultrasonicated suspension (5 mg catalyst, 16 µL Nafion perfluorinated resin solution (5 wt%), 250 µL isopropanol, and 750 µL water) and then dried in air at RT. The total catalyst loading was calculated to be 1.12 mg cm⁻². CV and LSV were recorded at a scan rate of 20 mV s⁻¹. The electrolyte was degassed thoroughly with Ar before measurement. All measured potentials were adjusted to NHE by adding 0.197 V. The overpotential is defined as $\eta = V_{\text{appl}} - E_{\text{ph}}$ without *iR* compensation, in which V_{appl} is the applied potential versus NHE and E_{ph} is the thermodynamic potential required for water oxidation at a certain pH [E_{ph} (V vs. NHE) = 1.23 V – 0.0592 pH].

Isotope-labeling experiment

An isotope-labeling experiment was performed following a literature procedure with some modification.^[60] H₂¹⁸O (2 mL, 97% enriched) and borate buffer solution (0.2 M, pH 8.0) that contained **2** (2 mg), [Ru(bpy)₃]²⁺ (1.0 mM), and K₂S₂O₈ (9.0 mM) was irradiated using a 450 nm LED lamp in a small tube sealed with a rubber plug after bubbling Ar. After 60 min, a portion (100 µL) of the gas in the headspace was injected into a mass spectrometer (MID, model; Omnistar/quadrupole mass analyzer; Pfeiffer Vacuum) with He (flow 30 mL min⁻¹) as the carrier gas for analysis. As a control experiment, H₂¹⁶O solution of borate buffer (2 mL, 0.2 M, pH 8.0) that contained **2** (2 mg), [Ru(bpy)₃]²⁺ (1.0 mM), and K₂S₂O₈ (9.0 mM) was put into a small tube sealed with a rubber plug. After flushing with Ar for 60 min, a portion (100 µL) of the gas in the headspace was sampled and analyzed as mentioned above. Three parallel experiments were performed for the isotope-labeling experiment, and the average data for each ion were used to calculate the net oxygen evolved and the ratio of ³²O₂/³⁴O₂/³⁶O₂ (Figure S16 and Table S2).

Acknowledgements

We gratefully acknowledge the Natural Science Foundation of China and Shandong Province (21402107, 91427303, 21571115 ZR2014BM011), fundamental research and subject construction funds, and Young Scholars Program of Shandong University (2015WLJH23).

Keywords: heterogeneous catalysis • metal–organic frameworks • oxygen • photochemistry • water splitting

- [1] a) D. G. Nocera, *Acc. Chem. Res.* **2012**, *45*, 767–776; b) N. S. Lewis, D. G. Nocera, *Proc. Natl. Acad. Sci. USA* **2006**, *103*, 15729–15735.
- [2] a) H. B. Gray, *Nat. Chem.* **2009**, *1*, 7; b) R. Eisenberg, H. B. Gray, *Inorg. Chem.* **2008**, *47*, 1697–1699.
- [3] M. D. Kärkäs, O. Verho, E. V. Johnston, B. Åkermark, *Chem. Rev.* **2014**, *114*, 11863–12001.
- [4] X. Sala, S. Maji, R. Bofill, J. García-Antón, L. Escriche, A. Llobet, *Acc. Chem. Res.* **2014**, *47*, 504–516.
- [5] F. Li, Y. Jiang, B. Zhang, F. Huang, Y. Gao, L. Sun, *Angew. Chem. Int. Ed.* **2012**, *51*, 2417–2420; *Angew. Chem.* **2012**, *124*, 2467–2470.
- [6] a) A. Magnuson, M. Anderlund, O. Johansson, P. Lindblad, R. Lomoth, T. Polivka, S. Ott, K. Stensjö, S. Styring, V. Sundström, L. Hammarström, *Acc. Chem. Res.* **2009**, *42*, 1899–1909; b) W. J. Youngblood, S.-H. A. Lee, K. Maeda, T. E. Mallouk, *Acc. Chem. Res.* **2009**, *42*, 1966–1973; c) W. Lubitz, E. J. Reijerse, J. Messinger, *Energy Environ. Sci.* **2008**, *1*, 15–31; d) L.-Z. Wu, B. Chen, Z.-J. Li, C.-H. Tung, *Acc. Chem. Res.* **2014**, *47*, 2177–2185.
- [7] a) S. Berardi, S. Drouet, L. Francas, C. Gimbert-Surinach, M. Guttentag, C. Richmond, T. Stoll, A. Llobet, *Chem. Soc. Rev.* **2014**, *43*, 7501–7519; b) A. M. Appel, J. E. Bercaw, A. B. Bocarsly, H. Dobbek, D. L. DuBois, M. Dupuis, J. G. Ferry, E. Fujita, R. Hille, P. J. A. Kenis, C. A. Kerfeld, R. H. Morris, C. H. F. Peden, A. R. Portis, S. W. Ragsdale, T. B. Rauchfuss, J. N. H. Reek, L. C. Seefeldt, R. K. Thauer, G. L. Waldrop, *Chem. Rev.* **2013**, *113*, 6621–6658.
- [8] a) D. Gust, T. A. Moore, A. L. Moore, *Acc. Chem. Res.* **2009**, *42*, 1890–1898; b) S. Fukuzumi, T. Suenobu, *Dalton Trans.* **2013**, *42*, 18–28; c) A. McSkimming, S. B. Colbran, *Chem. Soc. Rev.* **2013**, *42*, 5439–5488.
- [9] a) J. P. McEvoy, G. W. Brudvig, *Chem. Rev.* **2006**, *106*, 4455–4483; b) Y. Umena, K. Kawakami, J.-R. Shen, N. Kamiya, *Nature* **2011**, *473*, 55–60.
- [10] a) J. M. Lehn, J. P. Sauvage, R. Ziessl, *Nouv. J. Chim.* **1980**, *4*, 355–358; b) F. Jiao, H. Frei, *Angew. Chem. Int. Ed.* **2009**, *48*, 1841–1844; *Angew. Chem.* **2009**, *121*, 1873–1876; c) H. Junge, N. Marquet, A. Kammer, S. Denner, M. Bauer, S. Wohlrab, F. Gartner, M. M. Pohl, A. Spannenberg, S. Gladiali, M. Beller, *Chem. Eur. J.* **2012**, *18*, 12749–12758.
- [11] a) D. J. Wasylenko, R. D. Palmer, C. P. Berlinguet, *Chem. Commun.* **2013**, *49*, 218–227; b) R. Cao, W. Lai, P. Du, *Energy Environ. Sci.* **2012**, *5*, 8134–8157.
- [12] a) J. J. Concepcion, J. W. Jurss, M. K. Brenneman, P. G. Hoertz, A. O. T. Patrocino, N. Y. Murakami Iha, J. L. Templeton, T. J. Meyer, *Acc. Chem. Res.* **2009**, *42*, 1954–1965; b) J. J. Concepcion, M.-K. Tsai, J. T. Muckerman, T. J. Meyer, *J. Am. Chem. Soc.* **2010**, *132*, 1545–1557.
- [13] a) L. Wang, L. Duan, B. Stewart, M. Pu, J. Liu, T. Privalov, L. Sun, *J. Am. Chem. Soc.* **2012**, *134*, 18868–18880; b) L. Duan, F. Bozoglian, S. Mandal, B. Stewart, T. Privalov, A. Llobet, L. Sun, *Nat. Chem.* **2012**, *4*, 418–423.
- [14] D. J. Wasylenko, C. Ganesamoorthy, M. A. Henderson, B. D. Koivisto, H. D. Osthoff, C. P. Berlinguet, *J. Am. Chem. Soc.* **2010**, *132*, 16094–16106.
- [15] I. López, M. Z. Ertem, S. Maji, J. Benet-Buchholz, A. Keidel, U. Kuhlmann, P. Hildebrandt, C. J. Cramer, V. S. Batista, A. Llobet, *Angew. Chem. Int. Ed.* **2014**, *53*, 205–209; *Angew. Chem.* **2014**, *126*, 209–213.
- [16] H. Yamazaki, T. Hakamata, M. Komi, M. Yagi, *J. Am. Chem. Soc.* **2011**, *133*, 8846–8849.
- [17] N. Kaveevivitchai, R. Chitta, R. F. Zong, M. El Ojaimi, R. P. Thummel, *J. Am. Chem. Soc.* **2012**, *134*, 10721–10724.
- [18] Q. Zeng, F. W. Lewis, L. M. Harwood, F. Hartl, *Coord. Chem. Rev.* **2015**, *304*–305, 88–101.
- [19] R. Lalrempuia, N. D. McDaniel, H. Muller-Bunz, S. Bernhard, M. Albrecht, *Angew. Chem. Int. Ed.* **2010**, *49*, 9765–9768; *Angew. Chem.* **2010**, *122*, 9959–9962.
- [20] N. D. McDaniel, F. J. Coughlin, L. L. Tinker, S. Bernhard, *J. Am. Chem. Soc.* **2008**, *130*, 210–217.
- [21] a) J. D. Blakemore, N. D. Schley, D. Balcells, J. F. Hull, G. W. Olack, C. D. Incarvito, O. Eisenstein, G. W. Brudvig, R. H. Crabtree, *J. Am. Chem. Soc.* **2010**, *132*, 16017–16029; b) U. Hintermair, S. M. Hashmi, M. Elimelech, R. H. Crabtree, *J. Am. Chem. Soc.* **2012**, *134*, 9785–9795.

- [22] D. G. H. Hetterscheid, J. N. H. Reek, *Chem. Commun.* **2011**, *47*, 2712–2714.
- [23] A. Bucci, A. Savini, L. Rocchigiani, C. Zuccaccia, S. Rizzato, A. Albinati, A. Llobet, A. Macchioni, *Organometallics* **2012**, *31*, 8071–8074.
- [24] O. Diaz-Morales, T. J. P. Hersbach, D. G. H. Hetterscheid, J. N. H. Reek, M. T. M. Koper, *J. Am. Chem. Soc.* **2014**, *136*, 10432–10439.
- [25] a) J. Limburg, J. S. Vrettos, L. M. Liable-Sands, A. L. Rheingold, R. H. Crabtree, G. W. Brudvig, *Science* **1999**, *283*, 1524–1527; b) J. Limburg, J. S. Vrettos, H. Chen, J. C. de Paula, R. H. Crabtree, G. W. Brudvig, *J. Am. Chem. Soc.* **2001**, *123*, 423–430.
- [26] E. A. Karlsson, B. L. Lee, T. Åkermark, E. V. Johnston, M. D. Karkas, J. L. Sun, O. Hansson, J. E. Backvall, B. Åkermark, *Angew. Chem. Int. Ed.* **2011**, *50*, 11715–11718; *Angew. Chem.* **2011**, *123*, 11919–11922.
- [27] C. Zhang, C. Chen, H. Dong, J.-R. Shen, H. Dau, J. Zhao, *Science* **2015**, *348*, 690–693.
- [28] a) S. M. Barnett, K. I. Goldberg, J. M. Mayer, *Nat. Chem.* **2012**, *4*, 498–502; b) Z. Chen, T. J. Meyer, *Angew. Chem. Int. Ed.* **2013**, *52*, 700–703; *Angew. Chem.* **2013**, *125*, 728–731.
- [29] a) M.-T. Zhang, Z. Chen, P. Kang, T. J. Meyer, *J. Am. Chem. Soc.* **2013**, *135*, 2048–2051; b) X.-J. Su, M. Gao, L. Jiao, R.-Z. Liao, P. E. M. Siegbahn, J.-P. Chen, M.-T. Zhang, *Angew. Chem. Int. Ed.* **2015**, *54*, 4909–4914; *Angew. Chem.* **2015**, *127*, 4991–4996.
- [30] T. Zhang, C. Wang, S. Liu, J.-L. Wang, W. Lin, *J. Am. Chem. Soc.* **2014**, *136*, 273–281.
- [31] Q. Yin, J. M. Tan, C. Besson, Y. V. Geletii, D. G. Musaev, A. E. Kuznetsov, Z. Luo, K. I. Hardcastle, C. L. Hill, *Science* **2010**, *328*, 342–345.
- [32] D. K. Dogutan, R. McGuire, D. G. Nocera, *J. Am. Chem. Soc.* **2011**, *133*, 9178–9180.
- [33] D. J. Wasylenko, C. Ganesamoorthy, J. Borau-Garcia, C. P. Berlinguette, *Chem. Commun.* **2011**, *47*, 4249–4251.
- [34] C.-F. Leung, S.-M. Ng, C.-C. Ko, W.-L. Man, J. Wu, L. Chen, T.-C. Lau, *Energy Environ. Sci.* **2012**, *5*, 7903–7907.
- [35] M. L. Rigsby, S. Mandal, W. Nam, L. C. Spencer, A. Llobet, S. S. Stahl, *Chem. Sci.* **2012**, *3*, 3058–3062.
- [36] E. Pizzolato, M. Natali, B. Posocco, A. M. Lopez, I. Bazzan, M. D. Valentini, P. Galloni, V. Conte, M. Bonchio, F. Scandola, A. Sartorel, *Chem. Commun.* **2013**, *49*, 9941–9943.
- [37] a) H.-Y. Wang, E. Mijangos, S. Ott, A. Thapper, *Angew. Chem. Int. Ed.* **2014**, *53*, 14499–14502; *Angew. Chem.* **2014**, *126*, 14727–14730; b) H. Wang, Y. Lu, E. Mijangos, A. Thapper, *Chin. J. Chem.* **2014**, *32*, 467–473.
- [38] T. Nakazono, A. R. Parent, K. Sakai, *Chem. Commun.* **2013**, *49*, 6325–6327.
- [39] W. C. Ellis, N. D. McDaniel, S. Bernhard, T. J. Collins, *J. Am. Chem. Soc.* **2010**, *132*, 10990–10991.
- [40] J. L. Fillol, Z. Codola, I. Garcia-Bosch, L. Gomez, J. J. Pla, M. Costas, *Nat. Chem.* **2011**, *3*, 807–813.
- [41] Z. Codolà, I. Garcia-Bosch, F. Acuña-Parés, I. Prat, J. M. Luis, M. Costas, J. Lloret-Fillol, *Chem. Eur. J.* **2013**, *19*, 8042–8047.
- [42] M. K. Coggins, M.-T. Zhang, A. K. Vannucci, C. J. Dares, T. J. Meyer, *J. Am. Chem. Soc.* **2014**, *136*, 5531–5534.
- [43] B. Zhang, F. Li, F. Yu, H. Cui, X. Zhou, H. Li, Y. Wang, L. Sun, *Chem. Asian J.* **2014**, *9*, 1515–1518.
- [44] G. Chen, L. Chen, S.-M. Ng, W.-L. Man, T.-C. Lau, *Angew. Chem. Int. Ed.* **2013**, *52*, 1789–1791; *Angew. Chem.* **2013**, *125*, 1833–1835.
- [45] a) S. Fukuzumi, D. Hong, Y. Yamada, *J. Phys. Chem. Lett.* **2013**, *4*, 3458–3467; b) D. Hong, J. Jung, J. Park, Y. Yamada, T. Suenobu, Y.-M. Lee, W. Nam, S. Fukuzumi, *Energy Environ. Sci.* **2012**, *5*, 7606–7616.
- [46] a) Z. Huang, Z. Luo, Y. V. Geletii, J. W. Vickers, Q. S. Yin, D. Wu, Y. Hou, Y. Ding, J. Song, D. G. Musaev, C. L. Hill, T. Lian, *J. Am. Chem. Soc.* **2011**, *133*, 2068–2071; b) H. Lv, J. Song, Y. V. Geletii, J. W. Vickers, J. M. Sumliner, D. G. Musaev, P. Kögerler, P. F. Zhuk, J. Bacsa, G. Zhu, C. L. Hill, *J. Am. Chem. Soc.* **2014**, *136*, 9268–9271.
- [47] F. Song, Y. Ding, B. Ma, C. Wang, Q. Wang, X. Du, S. Fu, J. Song, *Energy Environ. Sci.* **2013**, *6*, 1170–1184.
- [48] X.-B. Han, Z.-M. Zhang, T. Zhang, Y.-G. Li, W. Lin, W. You, Z.-M. Su, E.-B. Wang, *J. Am. Chem. Soc.* **2014**, *136*, 5359–5366.
- [49] X.-B. Han, Y.-G. Li, Z.-M. Zhang, H.-Q. Tan, Y. Lu, E.-B. Wang, *J. Am. Chem. Soc.* **2015**, *137*, 5486–5493.
- [50] J. J. Stracke, R. G. Finke, *ACS Catal.* **2014**, *4*, 909–933.
- [51] A. R. Parent, R. H. Crabtree, G. W. Brudvig, *Chem. Soc. Rev.* **2013**, *42*, 2247–2252.
- [52] a) J.-L. Wang, C. Wang, W. Lin, *ACS Catal.* **2012**, *2*, 2630–2640; b) C. Wang, J.-L. Wang, W. Lin, *J. Am. Chem. Soc.* **2012**, *134*, 19895–19908; c) Z.-M. Zhang, T. Zhang, C. Wang, Z. Lin, L.-S. Long, W. Lin, *J. Am. Chem. Soc.* **2015**, *137*, 3197–3200.
- [53] T. Zhang, W. Lin, *Chem. Soc. Rev.* **2014**, *43*, 5982–5993.
- [54] T. Zhou, D. Wang, S. C.-K. Goh, J. Hong, J. Han, J. Mao, R. Xu, *Energy Environ. Sci.* **2015**, *8*, 526–534.
- [55] Y.-Z. Zheng, M.-L. Tong, W.-X. Zhang, X.-M. Chen, *Chem. Commun.* **2006**, 165–167.
- [56] Y. Han, Y. Wu, W. Lai, R. Cao, *Inorg. Chem.* **2015**, *54*, 5604–5613.
- [57] a) J. B. Gerken, J. G. McAlpin, J. Y. C. Chen, M. L. Rigsby, W. H. Casey, R. D. Britt, S. S. Stahl, *J. Am. Chem. Soc.* **2011**, *133*, 14431–14442; b) Y. Wu, M. Chen, Y. Han, H. Luo, X. Su, M.-T. Zhang, X. Lin, J. Sun, L. Wang, L. Deng, W. Zhang, R. Cao, *Angew. Chem. Int. Ed.* **2015**, *54*, 4870–4875; *Angew. Chem.* **2015**, *127*, 4952–4957; c) J. Han, D. Wang, Y.-H. Du, S. Xi, J. Hong, S. Yin, Z. Chen, T. Zhou, R. Xu, *J. Mater. Chem. A* **2015**, *3*, 20607–20613.
- [58] a) Y. Surendranath, D. A. Lutterman, Y. Liu, D. G. Nocera, *J. Am. Chem. Soc.* **2012**, *134*, 6326–6336; b) C. A. Kent, J. J. Concepcion, C. J. Dares, D. A. Torelli, A. J. Rieth, A. S. Miller, P. G. Hoertz, T. J. Meyer, *J. Am. Chem. Soc.* **2013**, *135*, 8432–8435.
- [59] A. I. Nguyen, M. S. Ziegler, P. Oña-Burgos, M. Sturzbecher-Hohne, W. Kim, D. E. Bellone, T. D. Tilley, *J. Am. Chem. Soc.* **2015**, *137*, 12865–12872.
- [60] C. Panda, J. Debogupta, D. Díaz Díaz, K. K. Singh, S. Sen Gupta, B. B. Dhar, *J. Am. Chem. Soc.* **2014**, *136*, 12273–12282.
- [61] a) L. Duan, Y. Xu, M. Gorlov, L. Tong, S. Andersson, L. Sun, *Chem. Eur. J.* **2010**, *16*, 4659–4668; b) L. Duan, Y. Xu, P. Zhang, M. Wang, L. Sun, *Inorg. Chem.* **2010**, *49*, 209–215.
- [62] a) M. Zhang, M. De Respinis, H. Frei, *Nat. Chem.* **2014**, *6*, 362–367; b) C. P. Plaisance, R. A. Van Santen, *J. Am. Chem. Soc.* **2015**, *137*, 14660–14672; c) H.-Y. Wang, S.-F. Hung, H.-Y. Chen, T.-S. Chan, H.-M. Chen, B. Liu, *J. Am. Chem. Soc.* **2016**, *138*, 36–39.

Received: January 25, 2016

Revised: March 6, 2016

Published online on April 21, 2016